
BACHELOR'S THESIS

# Experimental investigation of the excitation mechanism of a revolving gravity wave.

By

María Teresa Siles Campos,

Matr. Number 11741236

Carried out at the Institute of Fluid Mechanics and Heat Transfer (E322) of the Technischen Universität Wien.

Supervised by

Ao.Univ.Prof. Dipl.-Ing. Mag.rer.nat. Dr.techn. Herbert Steinrück.

Vienna, June 2018

# Abstract

Even though this experiment was already studied beforehand, some irregularities were found so in this new study some of them have been solved, and also in more realistic conditions as the testing bench has a size closer to the reality. The aim of this study of the excitation mechanism of a revolving gravity wave is to see how it behaves, how the wave develops among the time, how the amplitudes vary depending on some variables fixed and compare the results. The increasement of the amplitude versus the time and the decreasing of the number of waves rotating in the surface have been studied in three cases. Keeping as a constant during all the experiment the height difference between the calm water and the rotating disc above it, the speeds of 500, 600 and 700 revolutions per minute have been compared.

# Acknowledgements

To my family for giving me all their support, for making possible this five months out of home; to all the people that I have met here and that have made possible to me to feel like if home was not that far.

To Mr. Steinrück, who has guided me during this thesis and proposed me the subject to study. I thank him for his help and time whenever I needed him.

Special appreciation to Anton Maly, who was with me all the time at the laboratory, I knew I could count on him every time I needed. If it were not for him, this work would not have taken place.

Thank you too to people working at the workshop.

# Contents

# 1. Introduction.

Gravity waves are waves generated by the disturbance of a fluid subjected to the force of gravity as a restoring force. When a fluid is disturbed under the action of gravity and is moved away from its initial state of equilibrium, the fluid responds by forming waves that try to bring the system back to equilibrium.

In the experiment a partially water filled vertical cylinder of radius R induced by a rotating disc with an angular speed $\omega$. Above a critical angular velocity, a circulating gravity wave forms [1].

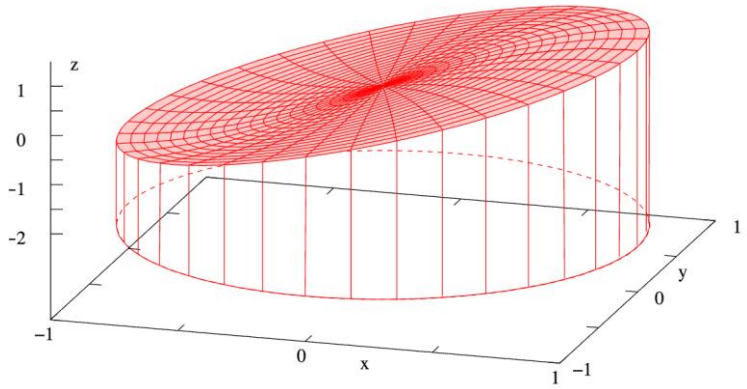


Figure 1: Potential flow solution equation.

Before starting the experiments, the aim of the project was settled. This time, we look at how the amplitude changes with time, and how the wave behaves in its different states and which patrons are repeated, how many waves are rotating at the same time in the surface of the water, so, the study is based on:

- How the amplitude variates with the time.
- How long takes the wave to reach its final and permanent state, and how it behaves trough the different intermediate states.
- Number of waves at any point of time.

These tests are done depending on a unique variable and maintain steady the rest of parameters. Every time the variable is changed, the test is repeated and discussed three or four times. The variable is:

- Speed (in r.p.m) of the motor.
- Height difference of the flat surface of the water and the rotating disc is kept constant and equal to 180mm.

# 2. Wave modes.

Sloshing means any motion of the free liquid surface inside its container. It is caused by any disturbance to partially filled liquid containers. Depending on the type of disturbance and container shape, the free liquid surface can experience different types of motion including simple planar, nonplanar, rotational, irregular beating, symmetric, asymmetric, quasi-periodic and chaotic. When interacting with its elastic container, or its support structure, the free liquid surface can exhibit fascinating types of motion in the form of energy exchange between interacting modes. Modulated free surface occurs when the free-liquid-surface motion interacts with the elastic support structural dynamics in the neighborhood of internal resonance conditions. Under low gravity field, the surface tension is dominant, and the liquid may be oriented randomly within the tank depending essentially upon the wetting characteristics of the tank wall. The basic problem of liquid sloshing involves the estimation of hydrodynamic pressure distribution, forces, moments and natural frequencies of the free-liquid surface. These parameters have a direct effect on the dynamic stability and performance of moving containers.

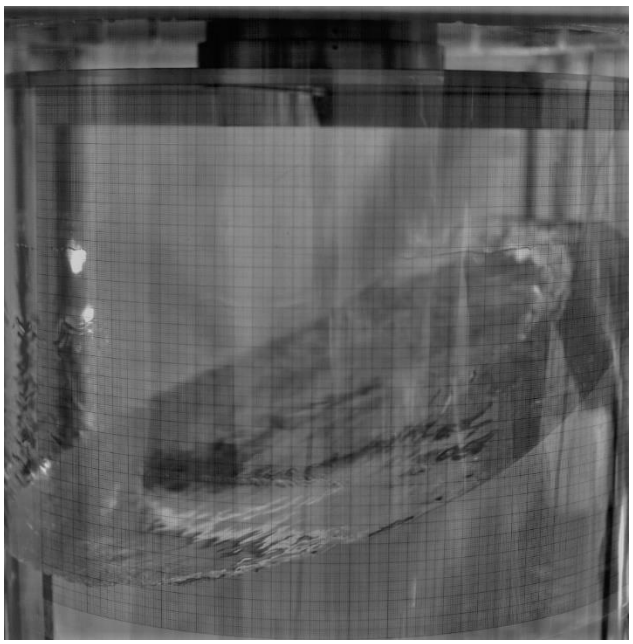

Figure 2: wave form.

A liquid's motion inside its container has an infinite number of natural frequencies, but it is the lowest few modes that are most likely to be excited by the motion of a vehicle. Most studies have therefore concentrated on investigating forced harmonic oscillations near the lowest natural frequencies, predicted by the fluid field linear equations. However, nonlinear effects result in the frequency of maximum response being slightly different from the linear natural frequency and dependent on amplitude. Nonlinear effects include amplitude jump, parametric resonance, chaotic liquid surface motion, and nonlinear sloshing mode interaction due to the occurrence of internal resonance among the liquid sloshing modes. The nonlinearities associated with free-surface motion inside moving containers are different from those nonlinear water waves in ocean and Canals.

The total velocity potential function, $\phi$, can be split into a disturbance potential function ($\tilde{\phi}$) and a potential function ($\phi_0$), in the form:

$$\phi = \tilde{\phi} + \phi_0 \tag{1}$$

For a bare wall cylindrical tank as shown in the picture Figure 3, a possible solution of the Laplace equation, which satisfies the wall and bottom boundary conditions listed in relations (2) and (3) which regards to the disturbance potential function ($\tilde{\phi}$), is (4) where $\alpha_{mn}$ and $\beta_{mn}$ are time dependent to be determined from the free-surface

$$\left.\frac{\delta\tilde{\phi}}{\delta r}\right|_{r=R} = 0 \tag{2}$$

$$\left.\frac{\delta\tilde{\phi}}{\delta z}\right|_{z=-h} = 0 \tag{3}$$

$$\tilde{\phi}(r,\theta,z,t) = \sum_{m=0}^{\infty}\sum_{n=1}^{\infty}\left[\alpha_{mn}(t)\cos m\theta + \beta_{mn}(t)\sin m\theta\right]J_m(\lambda_{mn}r)\frac{\cosh[\lambda_{mn}(z+h)]}{\cosh\lambda_{mn}h} \tag{4}$$

initial conditions, $J_m(\,)$ is the Bessel function of the first kind of order $m$, $\lambda_{mn}=\xi_{mn}/R$ are the roots of $\left.{}^{\delta J_m(\lambda_{mn}r)}/_{\delta r}\right|_{r=R} = 0$.

The analysis can be significantly simplified if the fluid field equations are linearized for small displacements. The normal mode frequencies are determined from the linearized free-surface boundary condition

$$\frac{\delta\tilde{\phi}}{\delta t} - g\eta = 0 \tag{5}$$

Differentiating once with respect to time and using equation $q = -\nabla\phi$ gives

$$\frac{\delta^2\tilde{\phi}}{\delta t^2} + g\frac{\delta\tilde{\phi}}{\delta z} = 0 \tag{6}$$

If the functions $\alpha_{mn}$ and $\beta_{mn}$ are expressed as harmonics, $\sin\omega_{m_n}t$, one can obtain the natural frequencies of the liquid free-surface by substituting equation (4) into (6)

$$\omega_{mn}^2 = \frac{g\xi_{mn}}{R}\tanh(\xi_{mn}h/R) \tag{7}$$

The above expression approaches a constant value for $h/R>2$, given by the following relation

$$\omega_{mn}^2 = \frac{g\xi_{mn}}{R}, \text{ for } \xi_{mn}h/R > 2.65 \tag{8}$$

If one considers surface tension, the linearized dynamic free-surface condition combined with the kinematic condition (6) gives, after using Laplace's equation,

$$\frac{\delta^2\hat{\phi}}{\delta t^2} + g\frac{\delta\tilde{\phi}}{\delta z} + \frac{\sigma}{\rho}\frac{\delta^3\hat{\phi}}{\delta z^3} = 0 \tag{9}$$

In this case the natural frequency is given by the expression

$$\omega_{mn}^2 = \left[\frac{g\xi_{mn}}{R} + \frac{\sigma\xi^3}{\rho R^3}\right]\tanh(\xi_{mn}h/R) \tag{10}$$

This result is valid for the slip contact line and it reveals that the surface tension causes an increase in the normal mode frequencies.

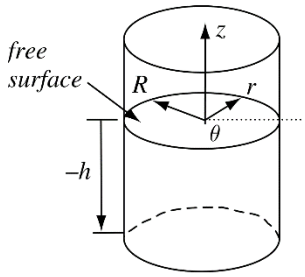


Figure 3: cylindrical container.

The fluid surface elevation $\eta$ measured from the undisturbed free surface is obtained from the equation (5) using (4)

$$\eta = \frac{1}{g}\sum_{m=0}^{\infty}\sum_{n=1}^{\infty}[\bar{\alpha}_{mn}\cos m\theta + \bar{\beta}_{mn}\sin m\theta]\,J_m(\lambda_{mn}r)\cosh(\lambda_{mn}h)(\omega_{mn}\cos\omega_{mn}t) \tag{11}$$

where $\bar{\alpha}_{mn}$ and $\bar{\beta}_{mn}$ are constant coefficients to be determined from initial conditions. The symmetric mode shape takes form

$$\eta(r,\theta,t) = \frac{1}{g}\sum_{m=0}^{\infty}\sum_{n=1}^{\infty}\bar{\alpha}_{mn}\cos m\theta\,J_m(\lambda_{mn}r)\cosh(\lambda_{mn}h)(\omega_{mn}\cos\omega_{mn}t) \tag{12}$$

For the first mode, $m = 0$, the motion is symmetric about the origin in the form of angular ridges and furrows. In this case, the roots of $dJ_0(\xi_{0n}r/R)/dr|_{r=R} = 0$ are $\xi_{0n}$=3.832, 7.0156, 10.173, …, $\pi(n + 0.25)$. The corresponding nodal circles are determined by setting $\eta = 0$, or $J_0(\xi_{0n}r/R) = 0$, which gives $\xi_{0n}r/R = 2.404, 5.517, 8.648, \ldots$ The corresponding radii of nodal circles are $r$ = 0.628$R$, 0.786$R$, 0.85$R$. [2]

# 3. Mathematical description.

To get an understanding of the mechanism of stimulation, the mathematical description will be discussed here. In the following chapters, however, this is done only for the orbiting gravity wave. The movement of the air, which is fanned by the rotating disk, is not explained in more detail. The resulting turbulent boundary layers, between air and disk and air and water surface, which are called Ekman layers, are not dealt with in this work.

## 3.1. Potential theory.

To describe the moving liquid, it is initially assumed that the surface tension and the friction forces on the cylinder wall are negligible. It is considered a liquid density $\rho$ in the gravitational field $g$, wherein in the equilibrium state, the surface is perpendicular to the gravitational acceleration.

In order to describe the observations mathematically, the potential theory is needed. To use this theory, it is still necessary to make the assumptions that the flow is incompressible and stationary. Due to the fact that no inflow takes place and the frictional forces on the cylinder wall are negligible, the flow is also free of vortices $(\omega = \nabla u = 0)$. Furthermore, according to the Helmholtz vortex theorems: "If a substantial fluid element is vortex-free, then it remains vortex-free for all times: $\omega\,(t = 0) = 0 \Rightarrow \omega\,(t > 0) = 0$."

For a simpler explanation, the more detailed connection of the potential theory in the x-y coordinate system will be dealt with below. The same considerations can also be applied to the cylindrical coordinate system, which will be used later to describe the rotating gravity shaft.

In order to solve the potential equation or Laplace equation, there must be a potential function $\Phi$ which satisfies the following two conditions. The partial derivative according to the x-coordinate must be equal to the velocity in the x-direction and the partial derivative of the y-coordinate must be equal to the velocity in the y-direction.

$$u_x = \frac{\delta \Phi}{\delta x}, u_y = \frac{\delta \Phi}{\delta y} \tag{13}$$

Substituting these two components (1) in the equation for vortex freedom

$$\frac{\delta u_x}{\delta x} - \frac{\delta u_y}{\delta y} = 0 \tag{14}$$

therefore, this is fulfilled:

$$\frac{\delta^2 \Phi}{\delta y \delta x} - \frac{\delta^2 \Phi}{\delta x \delta y} = 0. \tag{15}$$

The derivation of the equation for the condition of vortex freedom for a mass point $m$ is explained in detail in [5, pp. 222 - 224]. If one puts these two velocity components into the continuity equation as well

$$\frac{\delta u_x}{\delta x} + \frac{\delta u_y}{\delta y} = 0 \tag{16}$$

the potential equation or Laplace equation is obtained, which satisfies the differential equation of the vortex freedom.

$$\frac{\delta^2 \Phi}{\delta^2 x} + \frac{\delta^2 \Phi}{\delta^2 y} = 0. \tag{17}$$

With the Laplace operator, the equation for spatial flows is then

$$\Delta \Phi = 0. \tag{18}$$

In order to satisfy the continuity equation (4), a function $\Psi$, the current function, is searched for. Therefore, the speed components must satisfy the following condition.

$$u_x = \frac{\delta \Psi}{\delta y}, u_y = -\frac{\delta \Psi}{\delta x} \tag{19}$$

the second derivative is also fulfilled

$$\frac{\delta^2 \Psi}{\delta y \delta x} - \frac{\delta^2 \Psi}{\delta x \delta y} = 0. \tag{20}$$

If the velocity components are subsequently inserted into the equation for freedom from vertebrae (2), the differential equation of the current function is obtained

$$\frac{\delta^2 \Psi}{\delta^2 x} + \frac{\delta^2 \Psi}{\delta^2 y} = \Delta_2 \Psi = 0. \tag{21}$$

The lines at Ψ = constant represent the streamlines. The tangents at each point of these lines agree with the direction of the respective velocity vector. The lines at Φ = constant represent the potential lines.

## 3.2. Equations.

In this section, the equations already mentioned above are again written in cylindrical coordinates. According to the fundamental theorem of vector analysis it follows that one can express a vortex-free velocity field $\boldsymbol{u}\ (r, \varphi, z, t) = 0$ as velocity potential. The velocity field $\boldsymbol{u}$ has the following form in cylindrical coordinates

$$u = u\vec{e}_r + v\vec{e}_\varphi + w\vec{e}_z \tag{22}$$

Shown as potential results

$$u\ (r, \varphi, z, t) = \nabla \phi \tag{23}$$

Together with the continuity equation (∇u = 0) the potential equation follows

$$\nabla^2 \phi = 0 \tag{24}$$

With the Laplace operator, the Laplace equation in cylindrical coordinates is form

$$\Delta\phi = \frac{\delta\phi}{\delta r^2} + \frac{1}{r}\frac{\delta\phi}{\delta r} + \frac{1}{r^2}\frac{\delta\phi}{\delta\varphi^2} + \frac{\delta\phi}{\delta z^2} \tag{24}$$

## 3.3. Boundary conditions.

In order to be able to solve the Laplace equation (24), it is necessary to find boundary conditions for it. Initially, a cylindrical coordinate system is defined, with the origin of the coordinates being on the quiescent water surface and the z-axis pointing upwards. The first boundary condition is obtained by assuming that the radial velocity component of the wave at the edge of the cylinder must be zero.

$$\frac{\delta\phi(r=1)}{\delta r} = 0 \tag{25}$$

Furthermore, the speed in the z direction at the cylinder bottom is also zero. From this follows the second boundary condition with

$$\frac{\delta\phi(z=-h)}{\delta z} = 0 \tag{26}$$

To find a kinematic boundary condition, it is necessary to associate the vertical deflection of the surface with the velocity potential. With the assumption that every fluid element which was initially on the surface will also be on the surface at any later time, the equation can be written on the free surface with $z = h\ (r, \varphi, t)$. This means that the position in the $z$-direction depends only on the radial distance $r$, the angle $\varphi$ and the time $t$.

Deriving this equation over time, one obtains the velocity component $w$ in the $z$-direction.

$$\frac{\delta z}{\delta t} = w = \frac{\delta h}{\delta t} + \vec{u}\nabla\vec{h} = \frac{\delta h}{\delta t} + u\frac{\delta h}{\delta r} + v\frac{\delta h}{\delta\varphi} \tag{27}$$

$$w = \frac{\delta h}{\delta t} + u\frac{\delta h}{\delta r} + \frac{\dot{\varphi}}{r}\frac{\delta h}{\delta\varphi} \tag{28}$$

The dynamic boundary condition follows from the Bernoulli equation. If the pressure at the surface is equalized by $p = p_0$ and the time-dependent constant is drawn into the potential, the fourth boundary condition results

$$\frac{\delta\phi}{\delta t} + \frac{1}{2}\left(\left(\frac{\delta\phi}{\delta r}\right)^2 + \frac{1}{r^2}\left(\frac{\delta_\phi}{\delta\varphi}\right)^2 + \left(\frac{\delta\phi}{\delta z}\right)^2\right) + gh = 0 \tag{29}$$

## 3.4. Linearized problem.

To find the solution of the Laplace equation by means of the boundary conditions found above is not easy, since the boundary conditions contain several quadratic terms.

Assuming that the amplitudes are small compared to the radius $h << R$, the nonlinear quadratic terms are eliminated, and the linearized boundary conditions are obtained. The kinematic boundary condition on the surface is thus simplified

$$\frac{\delta\phi}{\delta z} = \frac{\delta h}{\delta t} \tag{30}$$

The dynamic boundary condition for $z = 0$ is now

$$\frac{\delta\phi}{\delta t} = -h \tag{31}$$

If you derive the latter again over time, you can equate it with equation (30) and you get

$$\frac{\delta\phi}{\delta z} + \frac{\delta^2\phi}{\delta t^2} = 0 \tag{32}$$

# 3.5. Product approach.

It is assumed that it is a rotating wave of immutable form, with the angular velocity $\omega$, which can be described by the following two equations.

$$\phi(r, z, \varphi, t) = a(r)Z(z)\sin(n\varphi - \omega t) \tag{33}$$

$$h(r, \varphi, t) = a(r)h_0\cos(n\varphi - \omega t) \tag{34}$$

Substituting these two equations for the shape of the wave into equation (32) gives the following relationship

$$\omega^2 = \frac{Z'(0)}{Z(0)} \tag{35}$$

This equation will be discussed later. To solve the Laplace equation, which is a partial differential equation with multiple variables, the product approach is used.

$$\phi = P(r)\phi(\varphi)Z(z) \tag{36}$$

$$\Delta\phi = P''\phi Z + \frac{1}{r}P'\phi Z + \frac{1}{r^2}P'\phi''Z + P\phi Z'' = 0 \tag{37}$$

$$P''\phi Z + \frac{1}{r}P'\phi Z + \frac{1}{r^2}P'\phi''Z + P\phi Z'' = 0$$

dividing by P

$$\frac{1}{P}\phi Z\left(P'' + \frac{1}{r}P'\right) + \frac{1}{r^2}\phi''Z + \phi Z'' = 0$$

Dividing by $\phi$

$$\frac{1}{P}Z\left(P'' + \frac{1}{r}P'\right) + \frac{1}{r^2}\frac{1}{\phi}\phi''Z + Z'' = 0$$

by Z

$$\frac{1}{P}\left(P'' + \frac{1}{r}P'\right) + \frac{1}{r^2}\frac{1}{\phi}\phi'' + \frac{1}{Z}Z'' = 0$$

Setting for $k = -\frac{1}{\phi}\phi''$ and $\mu = \frac{1}{Z}Z''$ you get the two differential equations

$$\frac{1}{\phi}\phi'' = -k \tag{38}$$

And

$$\frac{1}{Z}Z'' = \mu \tag{39}$$

$$Z'' - \mu^2 Z = 0$$

With the boundary condition that the velocity component on the ground must be zero $Z'(-h_w) = 0$, the solution for the differential equation is obtained

$$Z(z) = \frac{\cosh\left(\mu(z + h_w)\right)}{\cosh(\mu h_w)}$$

and thus the solution for equation (32)

$$\frac{Z'(0)}{Z(0)} = \mu \tanh(\mu h_w) = \omega^2 \tag{40}$$

The Laplace equation simplifies with the two variables *k* and $\mu$

$$\frac{1}{P}\left(P'' + \frac{1}{r}P'\right) - \frac{1}{r^2}k + \mu^2 = 0$$

multiplying by $\frac{P}{\mu^2}$

$$\frac{1}{\mu^2}\left(P'' + \frac{1}{r}P'\right) + P\left(1 - \frac{k}{r^2\mu^2}\right) = 0$$

Assuming the periodicity from the solution of the differential equation (38) sets you $k=n^2$

$$\frac{1}{\mu^2}\left(\frac{dP}{dr^2} + \frac{1}{r}\frac{dP}{dr}\right) + P\left(1 - \frac{n^2}{r^2\mu^2}\right) = 0$$

In the next step, $\mu r = x$ and $P(r) = \bar{P}(x)$ are set. Furthermore applies $\frac{1}{\mu}\frac{1}{dr} = \frac{1}{dx}$.

It follows

$$\frac{d\bar{P}(x)}{dx^2} + \frac{1}{x}\frac{d\bar{P}(x)}{dx} + \left(1 - \frac{n^2}{x^2}\right)\bar{P}(x) = 0$$

With $P(r) = \bar{P}(x) = J_n(x) = \bar{P}(\mu r) = J_n(\mu r)$ we obtain the Bessel function

$$J''_n + \frac{1}{r}J'_n - \frac{n^2}{r^2}J_n + J_n = 0 \tag{41}$$

With the boundary condition on the cylinder jacket (r = 1) follows

$$J_n'(\mu r) = 0$$

$$J_n'(\mu) = 0$$

# 3.6. Bessel function.

## 3.6.1. Introduction.

The problem of diffraction of plane waves from a circular cylinder of infinite extent has been solved both for electromagnetic and sound waves. Only slight modifications are necessary to obtain a corresponding solution for water waves incident on a circular pile. An exact mathematical solution is presented for the linearized problem of water waves of small steepness incident on a circular cylinder [3].

Bessel's equation arises when finding separable solutions to Laplace's equation and the Helmholtz equation in cylindrical or spherical coordinates. Bessel functions are therefore especially important for many problems of wave propagation.

In solving problems in cylindrical coordinate systems, one obtains Bessel functions of integer order ($\alpha = n$); in spherical problems, one obtains half-integer orders ($\alpha = n + 1/2$). In this paper we will describe the problem in cylindrical coordinates. Because this is a second-order differential equation, there must be two linearly independent solutions [4]. The fluid is frictionless. The ratio of the height of the waves to their length is sufficiently small so that all quantities involving the parameter (H/L) in the second or higher powers may be neglected without sensible error, thus giving rise to the so called linear theory. The waves are incident on a vertical circular cylinder which extends to the bottom. The depth of the water is finite [3].

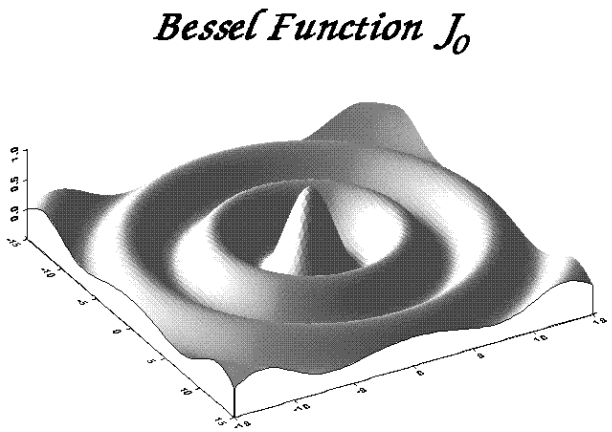


Figure 4: 3D illuminated grayscale surface of Bessel function order 0.

## 3.6.2. Bessel equation.

Bessel functions, first defined by the mathematician Daniel Bernoulli and then generalized by Friedrich Bessel, are the canonical solutions $u(x)$ of Bessel's differential equation.

In this section we will deal with the study of the ordinary differential equation

$$x^2u''(x) + xu'(x) + (x^2 - \alpha^2)u(x) = 0 \qquad (42)$$

with $\alpha \geq 0$, which is called the Bessel equation of order $\alpha$. It is an ordinary differential equation of order two with non-constant coefficients.

The solutions are the Bessel function of the first kind $J_{\pm\alpha}(x)$, of the second kind $Y_\alpha(x)$ (also called Weber's function), and of the third kind $H_\alpha(x)$ (Hankel functions). Each one is a regular function of $x$ throughout the $x$-plane cut along the negative real axis, and for a fixed $x \neq 0$ each is an integral function of $\alpha$. When $\alpha = \pm n$, $J_\alpha(x)$ has no Branch point and is an integral function of $x$.

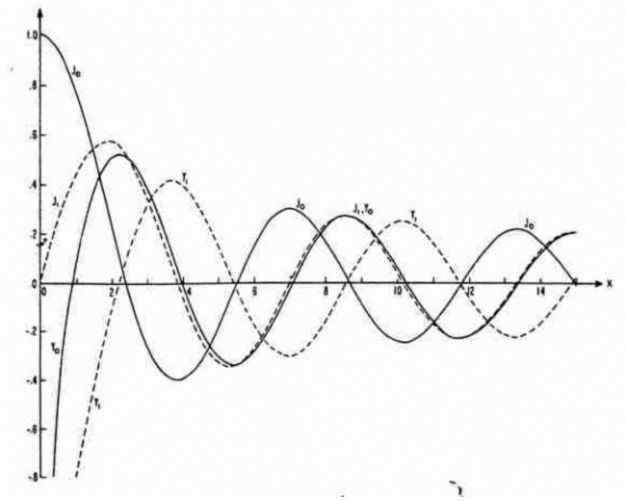

Figure 5: Bessel function of first and second kind $J_\alpha$ and $Y_\alpha$.

Bessel functions for integer $\alpha$ are also known as cylinder functions or the cylindrical harmonics because they appear in the solution to Laplace's equation in cylindrical coordinates.

To solve equation (42) we propose a solution that can be written in the form

$$u(x) = \sum_{m=0}^{\infty} a_m x^{m+b} \qquad (a_0 \neq 0) \qquad (43)$$

where the exponent $b$ and the coefficients $a_m$ must be calculated.

Substituting (43) in (42) and after doing some calculations it is arrived at that the function (44), which is denominated Bessel function of first kind $(\alpha)$, is the solution for the equation (42) [5].

The ordinary Bessel functions of order α, called simply functions of Bessel of order α are solutions of the Bessel equation. There are two simple ways of expressing the general solution of the Bessel differential equation with parameter α, which are associated with the ordinary Bessel functions of first and second kinds ($J_\alpha$ and $Y_\alpha$ respectively).

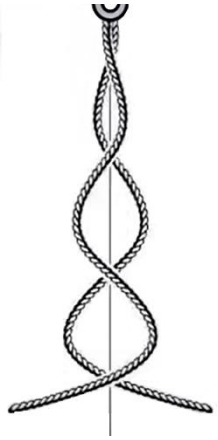

Figure 6: rotating chain takes the shape of the function $J_0$.

## 3.6.3. Bessel functions of the first kind: $J_\alpha$.

Bessel functions of the first kind, denoted as $J_\alpha(x)$, are solutions of Bessel's differential equation that are finite at the origin ($x = 0$) for integer or positive $\alpha$ and diverge as $x$ approaches zero for the negative non-integer $\alpha$. It is possible to define the function by its series expansion around $x = 0$, which can be found applying the Frobenius method to Bessel's equation:

$$J_\alpha(x) = \sum_{m=0}^{\infty} \frac{(-1)^m}{m!\,\Gamma(m+\alpha+1)} \left(\frac{x}{2}\right)^{2m+\alpha} \tag{44}$$

where $\Gamma(z)$ is the gamma function, a shifted generalization of the factorial function to non-integer values.

These functions comply with:

- If $\alpha \notin \mathbb{Z}$, then $J_\alpha(x)$ and $J_{-\alpha}(x)$ are linearly independent, and therefore a general solution of the Bessel equation can be expressed as a linear combination of them.
- If $\alpha = n \in \mathbb{Z}$, then it is fulfilled:

  $$J_{-n}(x) = (-1)^n J_n(x), \qquad \forall n \in \mathbb{Z}$$

  so the two solutions are no longer linearly independent. In this case, the second linearly independent solution will be a Bessel function of the second kind.

The graphs of Bessel functions look roughly like oscillating sine or cosine functions that decay proportionally to $1 / \sqrt{x}$ , although their roots are not generally periodic, but they are asymptotically for large values of $x$ [4].

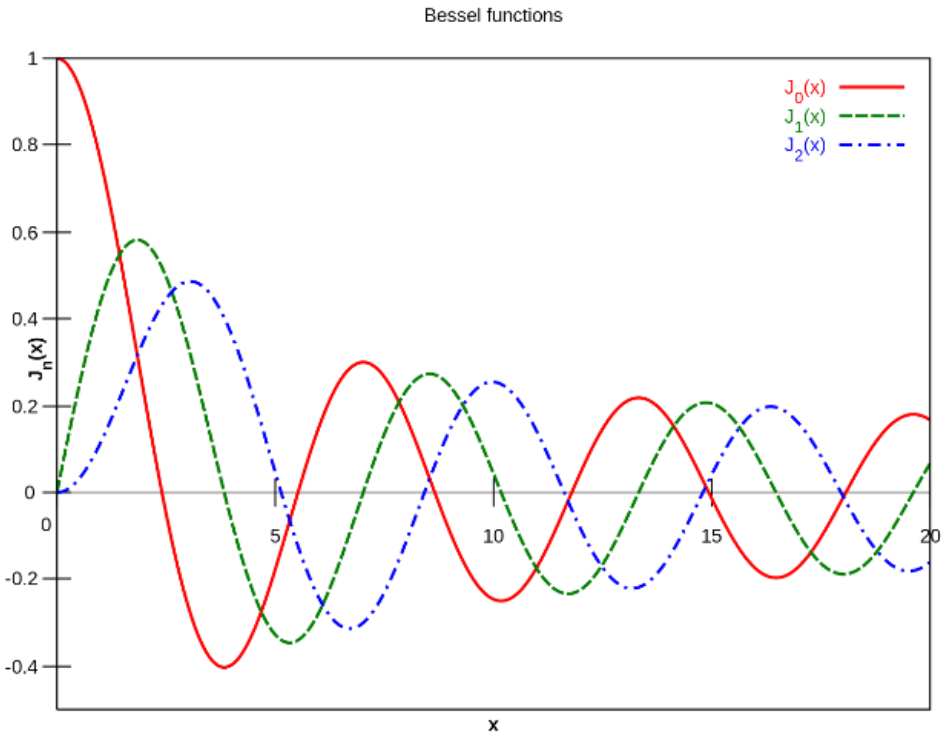


Figure 7: Plot of Bessel function of the first kind, $J_\alpha(x)$, for integer orders $\alpha$ = 0, 1, 2.

In the next table, the values for the roots of the derivative of the Bessel function are solved, thanks to NAG C Library, so that, the $x$ value for the maximums and minimums of the function for different values of $m$ are calculated:

| $\mu_{mk}$ | $k$=1 | 2 | 3 | 4 | 5 |
|---|---|---|---|---|---|
| $m$=1 | 1.8411853 | 5.3314457 | 8.5363183 | 11.706006 | 14.863590 |
| 2 | 3.0542342 | 6.7061352 | 9.9694694 | 13.170372 | 16.347523 |
| 3 | 4.2011847 | 8.0152380 | 11.345926 | 14.585849 | 17.788749 |
| 4 | 5.3175481 | 9.2823973 | 12.681909 | 15.964108 | 19.196030 |
| 5 | 6.4156109 | 10.519862 | 13.987189 | 17.312843 | 20.575515 |
| 6 | 7.5012605 | 11.734936 | 15.268182 | 18.637444 | 21.931716 |
| 7 | 8.5778307 | 12.932386 | 16.529366 | 19.941854 | 23.268054 |
| 8 | 9.6474158 | 14.115519 | 17.774013 | 21.229063 | 24.587198 |
| 9 | 10.711428 | 15.286738 | 19.004594 | 22.501399 | 25.891278 |
| 10 | 11.770871 | 16.447853 | 20.223032 | 23.760716 | 27.182022 |

Table 1: Zeroing the derivative of $J_\alpha$.

where *m* are the different values that $\alpha$ takes, and *k* the values in the *x-axis* when the derivative of $J_\alpha$ is made 0.

### 3.6.4. Bessel's integrals

For integer values of *n*, we have the following integral representation:

$$J_n(x) = \frac{1}{\pi}\int_0^{\pi} -\cos(n\tau - x\sin\tau)\,d\tau \tag{45}$$

That can also be written as:

$$J_n(x) = \frac{1}{2\pi}\int_{-\pi}^{\pi} e^{-i(n\tau - x\sin\tau)}\,d\tau \tag{46}$$

This was the approach that Bessel used, and from this definition he derived several properties of the function. This integral definition can be extended to non-integer orders by adding another integral term [4]:

$$J_\alpha(x) = \frac{1}{\pi}\int_0^{\pi} -\cos(\alpha\tau - x\sin\tau)\,d\tau - \frac{\lim(\alpha\pi)}{\pi}\int_0^{\infty} e^{-x\sinh(t)-\alpha t}\,dt \tag{47}$$

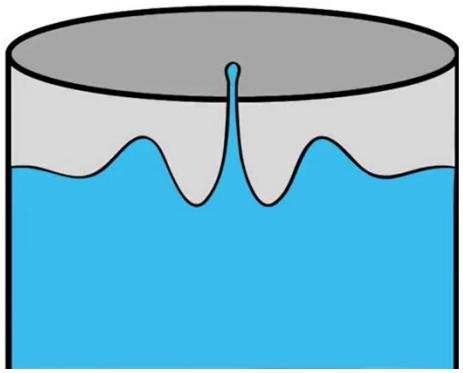

Figure 8: illustrative example of a wave taken the shape of the Bessel function of order 0.

# 4. Description of set-up.

## 4.1. Testing bench and cylinder.

All the necessary equipment is located at the laboratory of the Institute of Energy Technology and Thermodynamics, E302, and it's there where all the tests have been executed and studied. The testing bench was already installed there because it was used for other experiments years before. It consists on a structure formed by a plastic transparent cylinder held by steel bars whose dimensions are: height 102cm and ø40cm. In the bottom of the wall of the cylinder two holes are found, the first one is for the inlet of water, and next to it, another one for its outlet, both manipulated by manual valves in order to fill the cylinder with the exact amount of water. At the top of the cylinder there is a steel thick heavy disc fixed indirectly with screws in which the power unit is located. It is necessary to be careful with the pressures inside the cylinder since the disc is perfectly attached to the cylinder. Two extra holes were perforated during the experiments to introduce smoke into the bench (it is explained later).

This testing bench is used to simulate a pumping storage power plant in phase change operation in its simplest form. This allows us to observe and study the waves in simplified conditions.

A graph paper has been taped to the pipe on the outside on the front part. It has allowed us to measure the amplitudes in the photographs taken and also to determinate the initial level of the water.

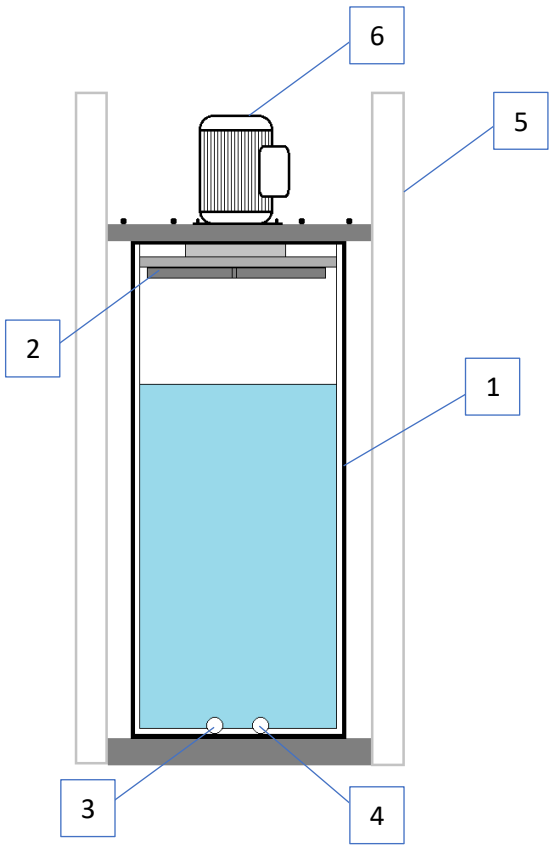


Figure 9: schematic representation of the experimental setup.

## 4.2. Propulsion.

Movement of water and so the creation of the waves inside the container is due to a rotating disc on top of it. This disc has a profile in "+" welded to him, and it rotates because of a motor screwed to it. This motor on the top of the external disc is connected to a standard inverter which also controls the nominal speed (in r.p.m.) of the motor. This frequency inverter is MOVITRAC® SEW EURODRIVE (4/U, 5/V, 6/W) and it's connected to the electrical network, in which we are able to choose the speed of the motor and also its direction of rotation. The motor rotates the disc inside the tube. The chosen motor is AEG , Typ AM 80 N2, (1,1Kw, cosφ=0,84, 4,7V, 2,7A, f=50Hz). The speeds of the motor are varied between 500 rpm and 700 rpm (in intervals of 100). We will see how the behavior of the wave changes depending on the speed. Initially the first speed to study was 400 rpm but it took too much time to form the wave, so we started to study from 500 rpm directly (and so we reach 700 rpm instead of 600).

| NUMBER | OBJECT | ADDITIONAL INFORMATION |
|---|---|---|
| **1** | ZYLINDER | Ø= 40 cm, height 102cm |
| **2** | ROTATING DISC | - |
| **3** | WATER INLET | - |
| **4** | WATER OUTLET | - |
| **5** | SUPPORT | Steel profiles |
| **6** | MOTOR | AEG, 1.1Kw, f=50Hz |

Table 2: Objects of the experimental setup.

## 4.3. Camera.

Figures 10 and 11: photo of Photron FASTCAM camera, and IMAGINGSOURCE camera.

To record the movements and behavior of the waves inside the cylinder we used the camera Photron FASTCAM Mini Ax 50, in which the objective NIKON, AF Nikkor 50mm, 1:1,4D. The camera was placed in a tripod in different positions in order to get the best view needed. At the beginning it was placed above the level of the inactive water and with a small angle, which made possible to focus on the hole top surface and take some pictures of the wave forms. After that, we approached the camera to the cylinder, we wanted to focus only the front part of it to make possible a better lecture of the

amplitudes. The videos recorded are a superposition of thousands black-and-white images, with a good resolution.

For a long time, it was tried to observe the development of the surface of the wave and its amplitudes not only in the borders of the cylinders, but also in the middle of the surface, crossing from side to side going through the center. For this, a laser was needed. Then the data could have been passed to a software and graphics could have been done. We tried a lot of settings to make it work, but the laser was not visible enough for the camera. We thought about making smoke inside the pipe, between the water surface and the rotating disc (taking care of the pressures inside) in order to make bigger the color differences between water surface and background. The smoke was generated first from a cigarette (a man smoking on a small plastic tube connected to the inside on the cylinder), then from incense sticks (they fitted in the small holes that the disc has, so it was possible to get the smoke inside), and finally with some pills makers of smoke, but they made so much smoke. None of these options were able to make the laser light seen through the camera.

The camera was controlled with the software provided by Photrom Fastcam Viewer, which allows many settings. The videos were filmed at the beginning at 500 fps (frames per second). Due to these high frame rates, very large files have already been created in a very short time, which consequently had long storage times (around 5 minutes each record) because the memory storage of the camera is small and the frames must be copied to the computer then. As it was necessary to film the whole development of the wave, it was necessary to add another camera, recording in parallel, whose storage is directly saved in the computer memory.

IMAGINGSOURCE DFK 23GP021 is the camera I'm talking about. It allowed us to save long videos directly in the computer through the software that was downloaded, IC CAPTURE 2.4. In parallel, the Photron FASTCAM was used to take pictures at singular moments. The resolution of this camera turned to be so low and the images recorded were useless. Besides, after recording some videos, the memory of the computer was full. All the data saved was deleted and start again.

The final setting we were looking for was finally was found in the FASTCAM software. Videos of 2 seconds were filmed in intervals of 15-23 seconds in the camera memory at 125fps.

## 4.4. Laser.

It was used for the firsts test we made. It was necessary to have the vision of the behavior of the wave in its complete form, as it was supposed to let us know the shape and amplitude of the wave right in the middle, not only in the borders. A support for the lent with the laser was necessary to be designed. This lent enabled to distort the light of the laser and make it perpendicular to the water surface, so the laser light illuminated the hole

surface. The light of the laser wasn't visible by its own, so it was necessary to manage some settings to make it more visible, as I explained before, making smoke was the thing we more studied, but we didn't get good results, so we leave the laser light out of the experiment. For a day we also try with a halogen light, but this was too weak and didn't make almost any effect.

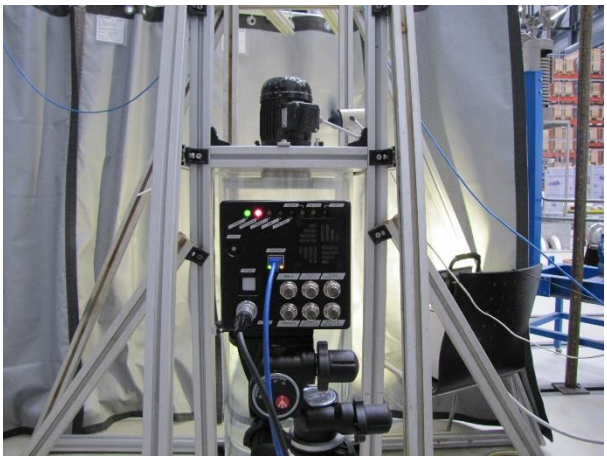

Figure 12: set-up

# 5. EXPERIMENTAL WORK AND DISCUSSION.

## 5.1. Study of the wave amplitude.

### 5.1.1. Realization and duration of recordings.

During the time spent in the laboratory, setting the FASTCAM camera and PHOTRON software took most of it. Trying different configurations such as the light (artificial and natural) and positions of the tripod also, was not an easy task as it depended on the environmental conditions and in the fact that every day the equipment had to be saved and so the next time it was necessary to start again. The fact that the memory of the camera was not enough for taking long recordings of the experiment slowed down the investigation, as it was not possible to proceed till the configuration needed was found. In the definitive position, the camera only focused in the front part of the cylinder, selecting the central line as the reference point for measure the amplitudes. The chronometer was located 2cm below the water reference line.

This was about recording short videos (2 sec) with an interval of about 15-20 secs between each one. The interval depended on the speed of the motor.

The instructions to follow were the following:

- Camera option: 1 Partition.
- Frames per second: 125fps (≈43 sec of recording in total).
- Trigger Mode // Random // number of frames: 250 frames.

- [View] // [Time-Lapse Bar] // ON // select Interval and Number of Repetitions.

The measurements depending on the rotation speed were:

-500 rpm: the time that the wave needed to develop itself completely was the longest one, so the intervals between records had to be longer to fit in the camera memory till the wave reached its maximum. The intervals were of 20 (tests 1, 2 and 3) and 25 secs (test 4).

-600 rpm: the maximum value of the amplitude was reached in a shorter time than with 500 rpm, which is obvious. We made one recording with intervals of 25sec between recordings to see if any discordance occurs after reaching the permanent mode. The following test were made in intervals of 17sec.

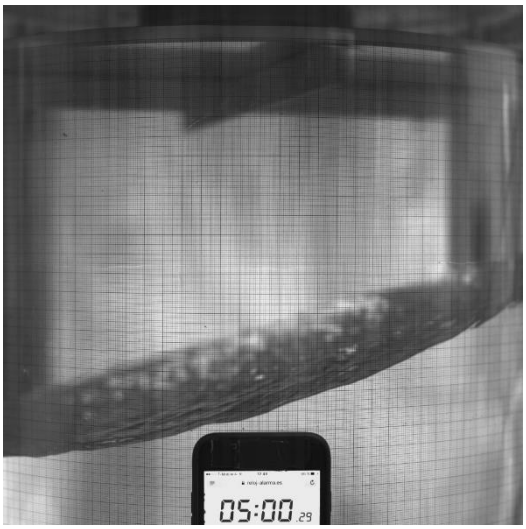


Figure 13: snapshot of the wave at 500 rpm.

-700 rpm: tests 1, 2 and 3 with intervals of 17 sec, and the last one, 13 sec, so we could take more intermediate points since anyways the water touched the disc quite some time before the video ended.

## 5.1.2. Analysis of the experiment.

The evaluation and study of the recordings was performed with the displayer of Windows 10, which allowed me to stop the video image by image whenever I wanted, so it was easy to measure the amplitudes in every instant. Also, it was easy to save single pictures from the videos.

A waiting time of 15 minutes was chosen between every recording. The chronometer and the recording of the video started simultaneously, and, around two seconds later, the motor started rotating. This was the faster I could press the button of the motor. It was necessary to assign the same time between the end and the beginning of each video, as the water on the bottom of the cylinder kept on moving despite the surface seemed standing. In this way, the initial conditions were as similar as possible in every test. For this reason, we discarded the first video of all, so there are only 3 videos at 500 rpm instead of 4.

The data taken from the videos at each speed are compiled in the following charts implemented in Excel, at different speeds.

The goal of these measurements is to see how the amplitude on the generated wave develops depending on the speed of the motor with a constant height difference (180mm).

The data was repeated 3 or 4 times per speed. We got the points enough for make the charts along the development of the waves.

In the chart (1), where the amplitudes at 500 rpm are described, we see almost a linear increase of the function. The amplitude gets bigger with the time at almost constant velocity, we don't see big jumps in the points taken. The final amplitude occurs at around 130mm as we can see in the Test 3, in which we took more time to measure. We can see that this amplitude gets constant from this value on in a time of 400 seconds. In any moment the wave reaches the rotating disc on the top. In test number 3, we can see that at the end, the amplitude decreases around 5 mm from the primary permanent state.

With the values picked for 600 rpm (chart (2)) we see that the waves increase faster than in the case before, reaching the height of 165mm in a time of 220 sec approx. Both in

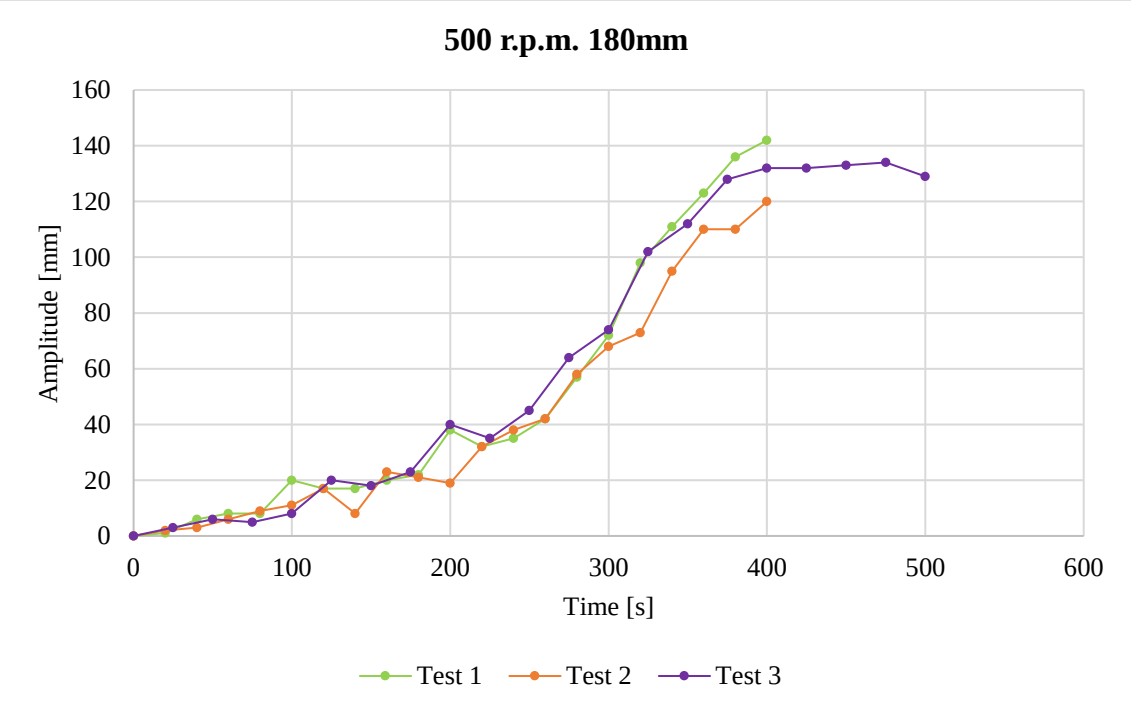


Chart 1: Amplitude vs Time, 500 rpm, 180mm.

600 and 700 rpm the total amplitude of the wave was not possible to see, since before achieving the permanent state, the wave touched the disc. At 700 rpm the top was reached at 150 seconds. The big change of the waves amplitude is between the time of 150 and 200 seconds for 600 rpm, and 125 to 150 seconds in the tests at 700 rpm, where the amplitude goes from 40 mm to 160mm, and from 80 mm to 170 mm, respectively.

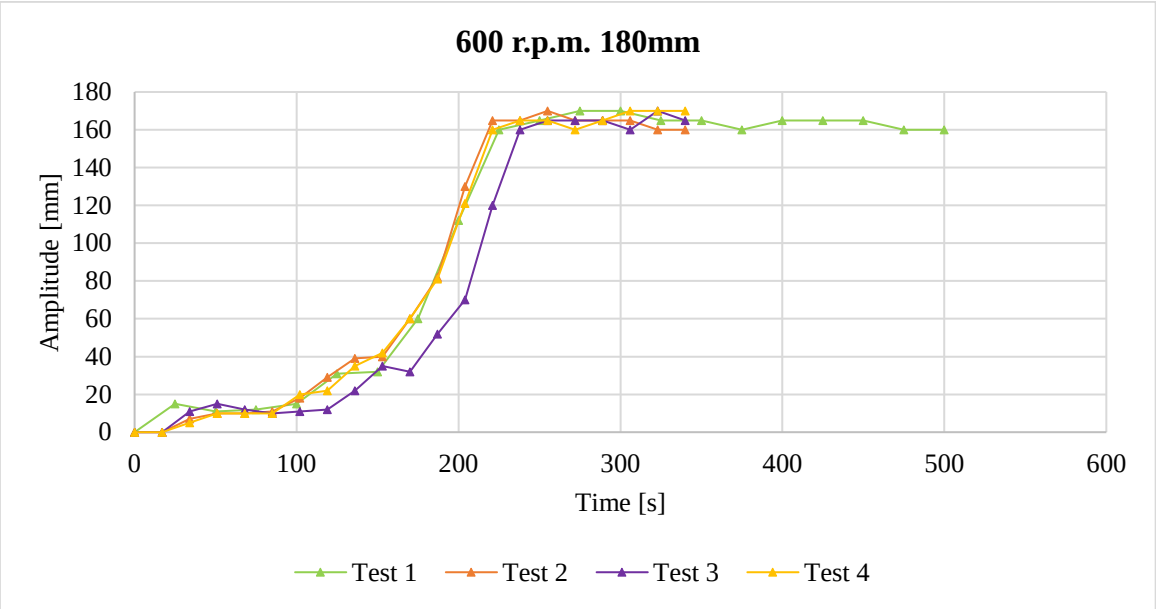


Chart 2: Amplitude vs Time, 600 rpm, 180mm.

In the last chart, the three speeds are compared. Three randomized tests have been chosen, one per speed. It can be clearly seen that, at lower speeds, the wave formation time is longer. There is not a big-time difference between 600 and 700 rpm to get the disc of the cylinder. The behavior of these two speeds is more similar comparing with the 500 rpm.

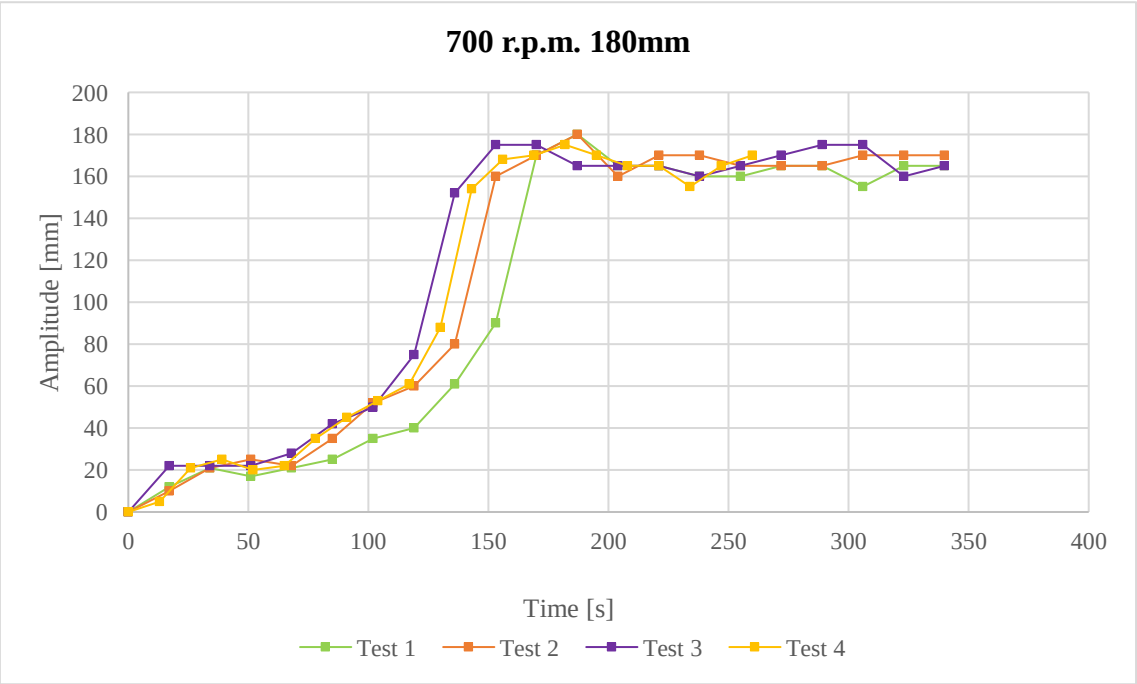


Chart 3: Amplitude vs Time, 700 rpm, 180mm.

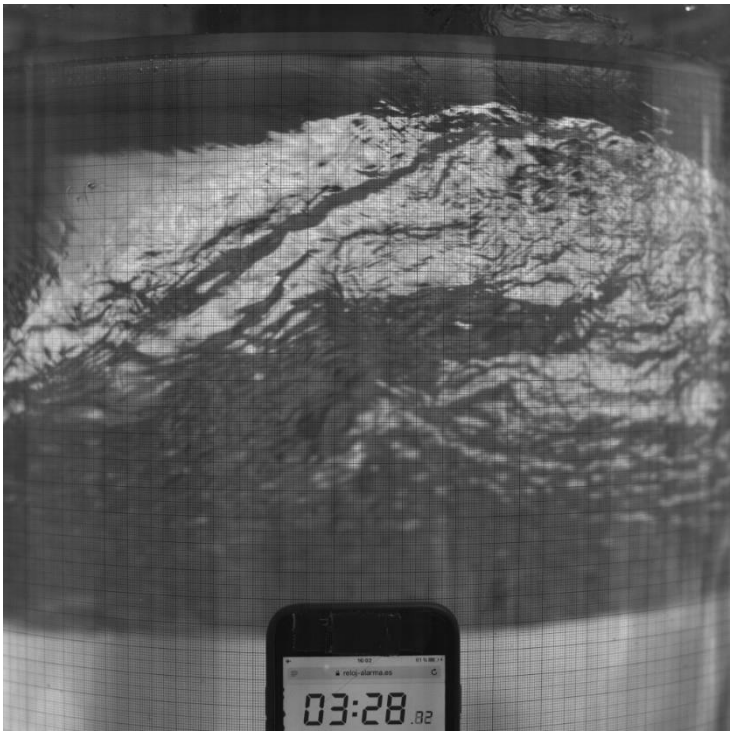


Due to the fact that the wave crashed with the profile of the disc, we can see some irregularities one the water reaches the amplitude of 165-175mm. The height at this point varies between 160 and 180 mm, since the profile has a measure of 20mm. on the video, we see that sometimes the water passed above the disc and splashed out on the surface above it.

Figure 14: we can see the water above the disc at a speed of 700rpm.

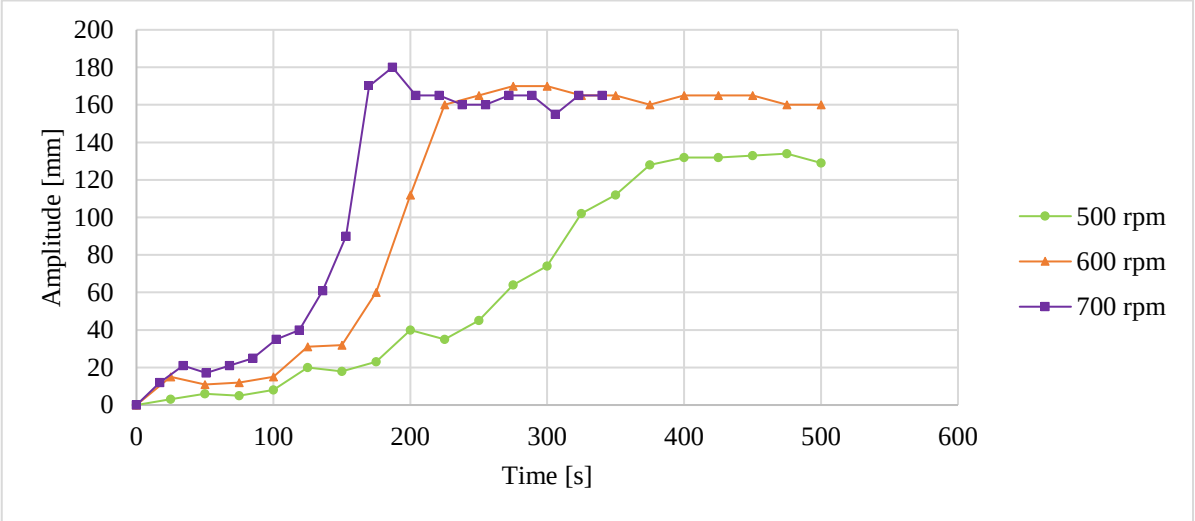


Chart 4: Amplitude vs Time. Comparison between 500, 600 and 700 rpm, 180mm.

## 5.2 Number of waves.

In this part of the thesis, the number of waves at every instant is going to be counted and their shapes described. The same videos that were used to measure the amplitudes in the previous section, have been used now to quantify the number waves in the surface of the water during the development of it till we can see a unique one. This last permanent wave occurs before the maximum amplitude is reached. In the charts we see that the number of waves decreases with the time. As the videos were recorded in intervals between 13 and 25, depending on the speed, as it was explained before, in the case of speed 500 rpm, where the wave takes shape in a longer time and also the intervals between videos is bigger, a big quantity of small waves was formed in the surface, which was complicated to count, so, in this case of 500 rpm, the method to get to the result was a rule of three. Assuming the periodicity of every wave, I counted how many waves were in the graph paper in the front part, measure how many millimeters they occupied and then divide the perimeter and multiply by the number of waves. Practical example given with the next picture.

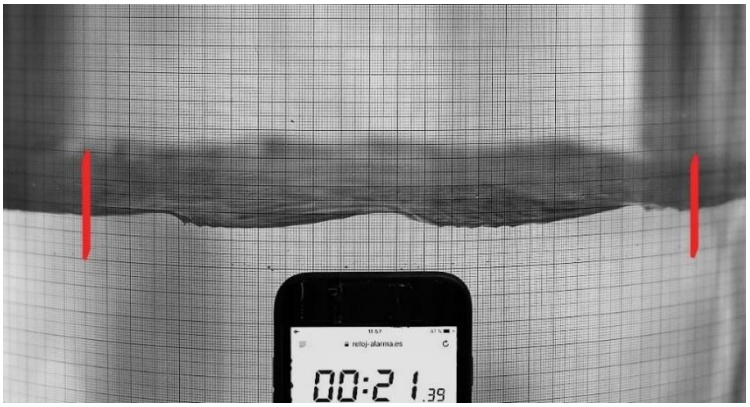


Figure 15: snapshot of Test 2 at 500 rpm.

In the strip between these two red lines three waves are visible. These three waves have a length in the perimeter of the cylinder of 25 cm, so, as it was said before, assuming the periodicity of every wave we have and assuming that this 3 waves are repeated every 25cm:

-cylinder perimeter: $2\pi R=2\pi \cdot 20=125'66$cm

- number of waves: 3

-length of all waves: 25 cm

So,

$$\frac{125'66}{25} \times 3 = 15'07 \approx 15 \text{ waves}$$

During the second snap of recording (at time 20sec approx.) we have around 15 waves in the surface of the water in this second test at 500 rpm. The same process was repeated por the rest of the trials at 500 rpm. This proceeding was not necessary for the tests at 600 and 700 rpm, because the wave was more developed by this time of 20 seconds and it was easy to count how many oscillations were quantitatively.

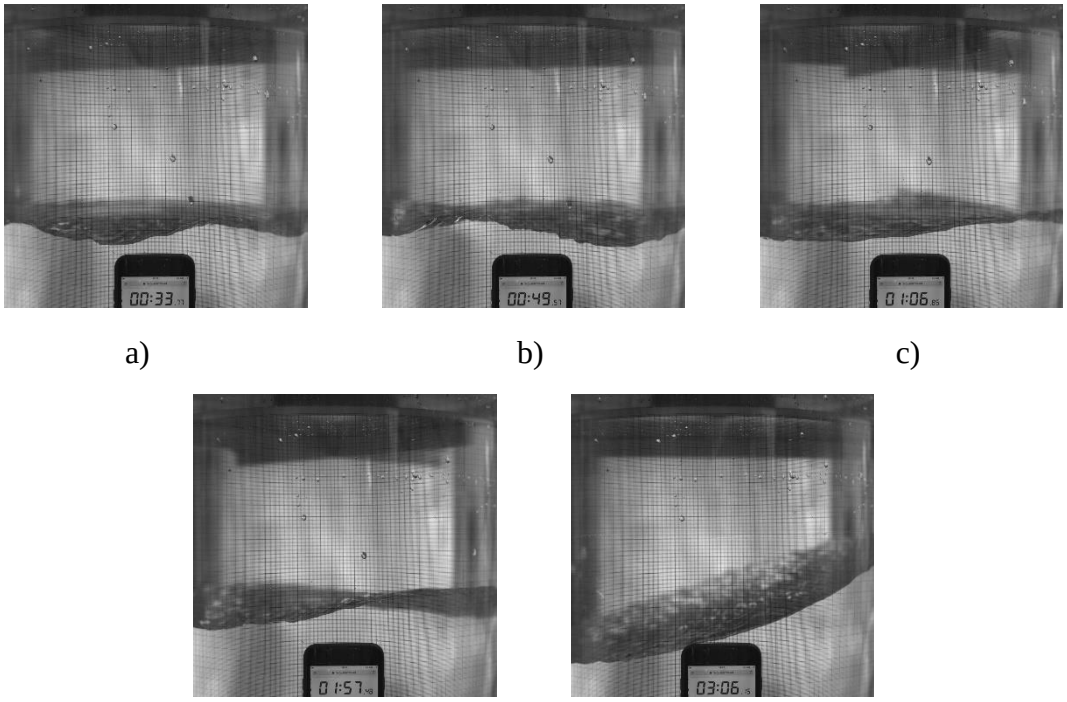

a) b) c)

d) e)

Figure 16: snapshots of a) 6, b) 5, c) 3, d) 2 and e) 1 wave. 600 rpm, 180mm.

Following charts show the number of waves per test depending on time.

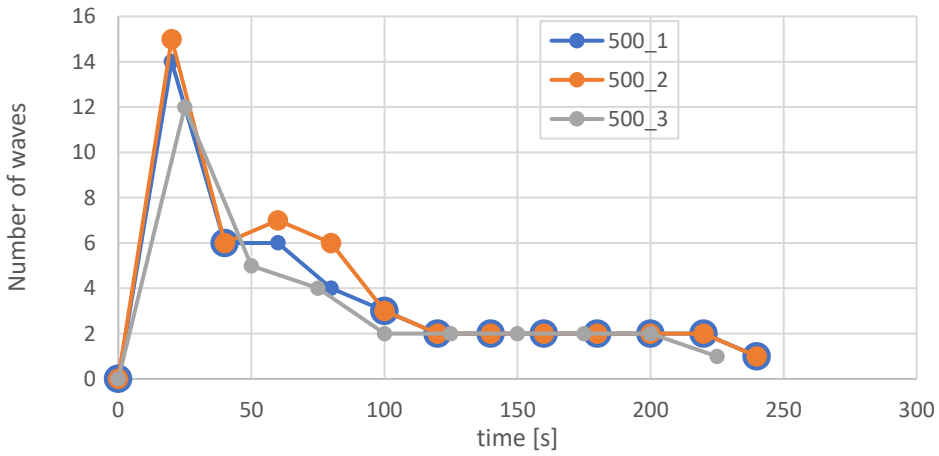


Chart 5: Number of waves vs Time, 500 rpm.

In the case of 600 rpm, in tests number 2, 3 and 4, the first-time shot was at 17 seconds and it was difficult to quantify the waves, as they were really small and irregular, so I skipped this 17 seconds point in the chart.

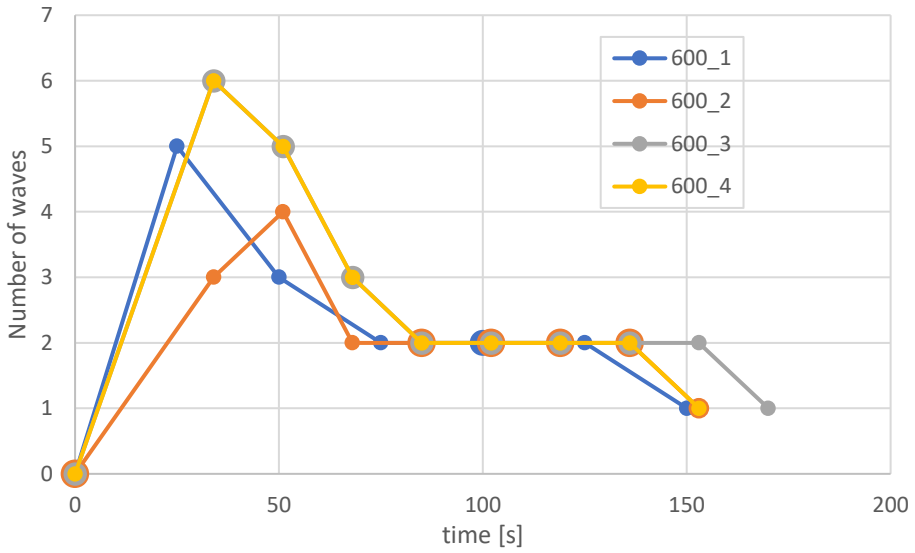


Chart 6: Number of waves vs Time, 600 rpm.

The time necessary to attain the last single wave depends on the speed. The higher the speed of the motor is, the sooner the single wave appears. It is possible to see that it happens at a time of 225 secs (500 rpm) and around 150 secs at 600 rpm. There are some irregularities in the experiment at 700 rpm. The last wave in this case appears at quite different values depending on the test. In test number 1 occurs at 136 secs, during the second, at 119 secs, and during the third and fourth attempt in a time of about 100 seconds.

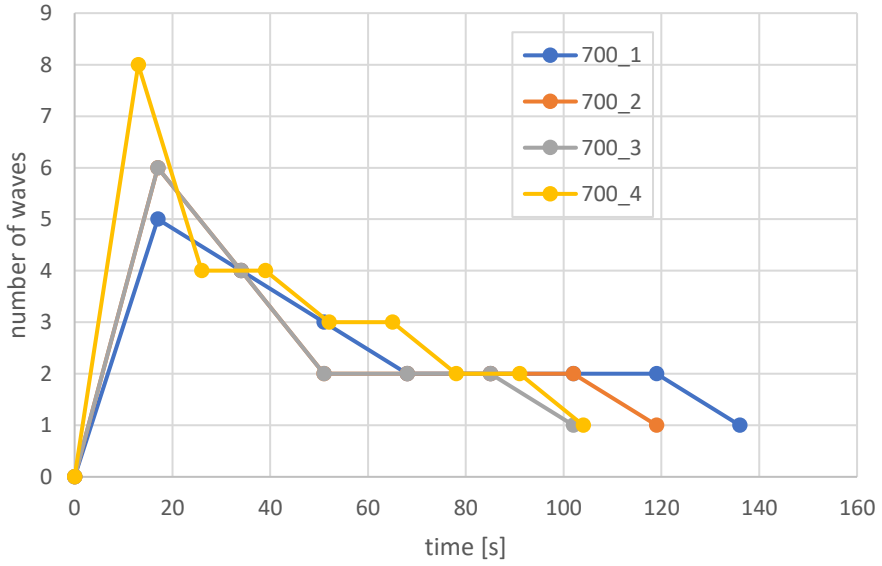


Chart 7: Number of waves vs Time, 700 rpm.

Once a single wave has been formed, it remains being one without exception. Without counting this case, the mode that takes the most time is when two waves are rotating in the surface of the water inside the cylinder. This time is also bigger when smaller is the speed: at 500 rpm, two waves behave playing for 150 seconds; at 600, around 60 seconds and, at 700, depending on the case, barely 40 seconds.

The jumps in the number of waves are more abrupt at 500 rpm, where we can see that in a time of 20 seconds, the number decreases from 15 waves to six. This does not happen in the last experiment, at 700 rpm, where at second 17 there are 5 waves, and seventeen seconds later we have only one less (test 1, 700 rpm).

# 6. Bibliography

[1] Steinruck H. und Gusner L.: *A circulating gravity wave in a cylindrical tank.* PAMM · Proc. Appl. Math. Mech. 15, 521 – 522 (2015). https://onlinelibrary.wiley.com/doi/epdf/10.1002/pamm.201510251

[2] Rouf A. Ibrahim (May 2005): *Liquid Sloshing Dynamics: Theory and Applications*. Wayne State University, Michigan: Cambridge, pp. 12-14.

[3] *Wave forces on piles: a diffraction theory*, December 1954. p. 6.

http://www.dtic.mil/dtic/tr/fulltext/u2/699406.pdf

[4] Wikipedia, Bessel function. https://en.wikipedia.org/wiki/Bessel_function

[5] Chapter 7: *Funciones de Bessel y su aplicación a la resolución de EDPs*, pp. 86-87.

http://filemon.upct.es/~fperiago/apuntes_docencia/tema7.pdf